EXPERIMENTAL ANALYSIS ON P-WAVE ATTENUATION IN CARBONATE ROCKS AND RESERVOIR IDENTIFICATION

JING BA[1], LIN ZHANG[1], DING WANG[2], ZHENYU YUAN[1], WEI CHENG[1], RUPENG MA[1]and CHUNFANG WU[1]

[1] *School of Earth Sciences and Engineering, Hohai University, Nanjing 211100, P.R. China.*
[2] *Center of Rock Mechanics and Geohazards, Shaoxing University, Shaoxing 312000, P.R. China. wdgeophysics@hotmail.com*

(Received June 29, 2017; revised version accepted June 9, 2018)

ABSTRACT

Ba, J., Zhang, L., Wang, D., Yuan, Z., Cheng, W., Ma, R. and Wu, C.F., 2018. Experimental analysis on P-wave attenuation in carbonate rocks and reservoir identification. *Journal of Seismic Exploration*, 27: 371-402.

Understanding the relationships between seismic wave responses and rock properties is a key factor for quantitative seismic interpretation and characterization of complex hydrocarbon reservoirs. We have performed laboratory ultrasonic measurements on 10 carbonate samples and recorded the waveforms under different conditions, such as varying pore-fluid types, confining and pore pressures and partial saturations. P- and S-wave velocities are measured on the basis of the first arrivals and the attenuation of P-waves is estimated by use of the spectrum-ratio method on the transmitted signals. The sensitivity analysis based on the experimental results show that P-wave attenuation is one of the most sensitive indicators for rock porosity and permeability, especially for low porosity rocks. P-wave attenuation is then used to identify the high quality carbonate reservoirs from the actual stratum on the basis of the post-stack seismic data. The inverse quality factor Q^{-1} is estimated by using the spectral ratio method based on a generalized S-transform of the post-stack seismic data. The empirical relations between porosity, permeability and P-wave attenuation, which are derived from the experimental measurements, are then applied to the values obtained from seismic profile. We predict the reservoir porosity and permeability from the carbonate stratum. The prediction results are in good agreement with the well log production reports, validating P-wave attenuation as an effective indicator for directly characterizing in-situ carbonate reservoirs.

KEY WORDS: attenuation, experimental measurement, reservoir identification, carbonate, rock physics, saturation, porosity, sensitivity.

0963-0651/18/$5.00

INTRODUCTION

As one of the most important hydrocarbon resources, carbonate reservoir rock holds more than 60% of the world's petroleum reserves and accounts for almost 40% of the world's total hydrocarbon production (Chopra et al. 2005). Carbonate is always a focus of the industrial exploration and production of oil and gas, and a hot spot of relevant studies. Carbonate rocks are mainly composed of two kinds of minerals, calcite and dolomite. Because of the littoral environments where they were produced, most carbonate rocks generally experienced multiple diagenesis and reformation effects in the long geologic history, resulting in the high complexity of texture, pore shape and structures in comparison with clastic rocks. Generally, the hydrocarbon exploration of carbonate reservoirs are more difficult than that of clastic reservoirs (Mahbaz et al., 2012). The factors which affect the seismic response, such as mineral composition, porosity, permeability and pore fluid saturation, are analyzed in rock physics tests and theoretical modeling, so as to bridge the gaps between a geologic description and seismic interpretation. Concerning carbonate reservoirs with high complex fabric structures, more attention should be paid to rock-physics studies so that a comprehensive interpretation can be made with rock tests, sonic logs and seismic imaging.

Acoustic velocity is one of the most important quantity in rock physics and seismic exploration, which is mainly controlled by the mineral grain, rock skeleton, porosity, pore shape, permeability, etc. However, in the long geologic diagenesis history, mostly carbonate rocks experienced complicated cementation, crystallization and dissolution processes, which changed the original rock skeleton and pore spaces. P- and S-wave velocities (V_P and V_S) in carbonate rocks with approximately the same porosity usually have large distribution ranges, making it difficult the precise identification of hydrocarbon reservoirs (Baechle et al., 2008). For instance, Eberli et al., (2003) performed rock physical measurements on carbonate samples from the Great Bahama Bank and analyzed the influence of porosity and pore shape on P- and S-wave speeds. Based on laboratory measurements, Sayers (2008) discussed the effects of pore shape variations on acoustic wave speeds and elastic moduli in carbonate rocks. Due to the differences in pore structure and pore size, Sun (2004) found P-wave speed are different in the two rocks of the same porosity and different permeability. Weger et al. (2009) analyzed the effect of pore structure on sonic velocity and permeability in carbonates by introducing a digital image analysis method.

The differential effective medium (DEM) theory, in which pore shapes are assumed to be ellipsoids with different aspect ratios, was applied to establish a relationship between pore shapes and wave velocities in carbonates (Kumar and Hang, 2005; Baechle et al., 2008; Sun et al., 2012). The results showed that the elastic wave velocities in carbonate rocks are

very sensitive to the compliant flat pores, such as micro-cracks and fractures. Sain et al. (2008) sorted the pores of carbonate into three categories of rigid pores, inter-granular pores and cracks, and used the Xu-White model (Xu and White, 1995), which is originally developed for the studies in clastic rocks, to calculate the acoustic wave velocities. Xu and Payne (2009) extended the Xu-White model, and obtained the volume contents of the soft pores and the stiff pores in carbonate rocks, respectively, by using the inversion of wave velocities.

Pore-fluids significantly affect the elastic wave propagation characteristics in carbonate rocks. Prasad et al. (2005) analyzed log data from the six wells to investigate the differences between oil-saturated and brine-saturated carbonate formations and derived the corresponding seismic responses. Gassmann's theory is commonly used in calculating the effective modulus and wave velocities of the fluid-saturated rocks. It is based on the assumption that the wet-rock shear modulus is equal to the dry-rock shear modulus. By performing laboratory measurements on 30 limestone samples from Cretaceous and Miocene carbonate reservoirs, with porosity ranging from 5 % to 30 % with varying textures and pore types, Baechle et al. (2005) observed that the shear modulus decreases after water was injected into the rocks. Comparing the measured S-wave velocities of a set of carbonate rocks with those computed by Gassmann's theory, Vanorio et al. (2008) found that the experimental modulus is lower than the predicted one. They suggested that some alteration mechanisms such as dissolution, cementation, recrystallization, and replacement by newly-formed phases may result in deviations from Gassmann's theory.

Due to the effect of pore shape, mineral composition, fabric structure and fluid type, the P-wave velocity of carbonate rocks varies in a wide range for the same porosity. To identify carbonate reservoirs with post-stack seismic data can be problematic, if it is only based on P-wave velocity. On the other hand, wave attenuation is an important indicator in seismic exploration. It is even more effective than wave velocity, since generally seismic waves will undergo strong attenuation in fluid-saturated porous strata (e.g., Ba et al., 2015). Laboratory experiments and theoretical studies (White, 1975; Mavko and Nur, 1979; Winkler and Murphy, 1995; Pride et al., 2004; Adam et al., 2009; Ba et al., 2012, 2017; Bouchaala et al., 2014) showed that seismic attenuation is highly affected by porosity, fluid type and partial saturation. Winkler et al. (1979) showed that wave attenuation is much more sensitive to changes of fluid saturation than wave velocities. Dasgupta and Clark (1998) analyzed field data and concluded that attenuation can be used to distinguish rock lithology.

Seismic attenuation caused by the wave-induced local fluid flow mechanisms strongly depends on rock fabric heterogeneity and patchy saturation of immiscible fluids. Mavko and Nur (1975) proposed a squirt-flow model describing the local fluid flow mechanism between thin cracks and stiffer pores. Pride and Berryman (2004) presented the

double-porosity model, by considering local fluid flow between the two pore systems with different compressibilities. White (1975) and Carcione et al. (2003) investigated the local fluid flow's effects on attenuation by analyzing the geometric distribution of pore fluids. Ba et al. (2017) gave a double double-model by incorporating the effects of patchy saturation and rock fabric heterogeneity in the same poroelasticity framework.

In this work, we measure the ultrasonic wave velocity and attenuation of carbonate samples under the different conditions with varying pore-fluid type, confining pressure and hydrocarbon saturation. Compressional wave attenuation is estimated by use of a spectral-ratio method. The experimental data are analyzed and we test the sensitivity of the rock physics indicators to reservoir porosity and permeability. The seismic attenuation attributes are obtained from the post-stack data in the work area and the reservoirs are identified by applying the empirical relationships obtained from the experimental measurements.

EXPERIMENT MEASUREMENTS AND RESULTS

Carbonate rock samples

The laboratory experiments are performed on 10 samples from Tarim Basin of Northwest China to acquire the ultrasonic P- and S-waveforms in rock samples at in-situ conditions, whose properties are listed in Table 1. Samples A1, A2, B1, B2 and D are collected from the Ordovician formations of the H field, Tarim Basin of west China. Rocks from the target formation are mainly grey sparite and micritic limestone with very low porosity and permeability. Minerals are calcite and rare clay. Samples E1, E2, E3, F1 and F2 are collected from the Cambrian formations, Tarim Basin.

Table 1. Properties of carbonate rock samples.

Lithology		Dry-Rock Density (g/cm^3)	Porosity (%)	Permeability (mD)
Limestone	A1	2.67	1.37	0.068
	A2	2.63	1.12	0.051
	B1	2.65	1.63	0.006
	B2	2.67	0.71	1.559
	D	2.66	2.50	0.023
Dolomite	E1	2.69	5.10	0.091
	E2	2.66	5.34	0.458
	E3	2.67	5.47	0.174
	F1	2.41	12.08	162.753
	F2	2.44	12.28	22.819

Composed of almost pure dolomite, rocks from the formation are light-grey reef dolomite and granular dolomite with dissolved pores. In the samples, F1 has a relatively high permeability, which can be related to the embedded micro-fractures in the main carbonate skeleton. The in-situ confining pressure and temperature of the two formations are approximately 80MPa and 140°C, respectively. The depth of the formations is more than 4km from surface.

Experiment set-up

The carbonate samples are cut in cylindrical shapes (diameter 25.2 mm and length < 30 mm). The transmitting and receiving transducers are located at the two ends of the sample and the wave travel path is axial.

We used the experimental set-up of Guo et al. (2009), which is composed of a digital oscilloscope (Tektronix TDS420 A), a pulse generator (Panametrics 5077PR), a high pressure vessel, a temperature control unit, a confining pressure (P_c) control unit, a pore pressure (P_p) control unit and the acoustic testing unit. Based on the normal and shear vibrations, PZT (Piezoelectric Ceramic Transducer) is used to generate mainly P- and S-waves, respectively. The receiving transducer is connected to the PC through a signal amplifier. The wave measurement frequency is 1 MHz. The acquisition frequency for ultrasonic waveforms is 50 MHz and time sampling interval is 0.02 μs.

Measurements are performed on the 10 rock samples at full-water, full-oil (kerosene) and full-gas (nitrogen) saturation states, respectively, at a confining pressure of 80 MPa, pore pressure of 10 MPa, and temperature of 140°C. Waveforms are also measured at a varying confining pressure of 20-80 MPa with constant pore pressure of 10 MPa and temperature of 140°C.

Partial-saturation experiments are performed on the 5 dolomite samples with relatively high porosity at confining pressure of 80 MPa, pore pressure of 10 MPa, and temperature of 20°C. We used the method of Ba et al. (2016) to change the hydrocarbon saturation in those tested rocks. In the experiments with gas and water saturation, the sample was first fully saturated with water by a depressurizing method (using the digital pump) and then placed in a drying oven at more than 120°C to vary the water saturation. The best control of water saturation was achieved by weighing the sample. The sample was sealed with a rubber jacket and put in the vessel, and the confining pressure was increased to 80 MPa. Nitrogen was injected to achieve a pore pressure of up to 10 MPa. We maintained the temperature for half an hour and began ultrasonic measurements. With oil and water saturation, the sample was fully saturated with oil and then dried in the oven

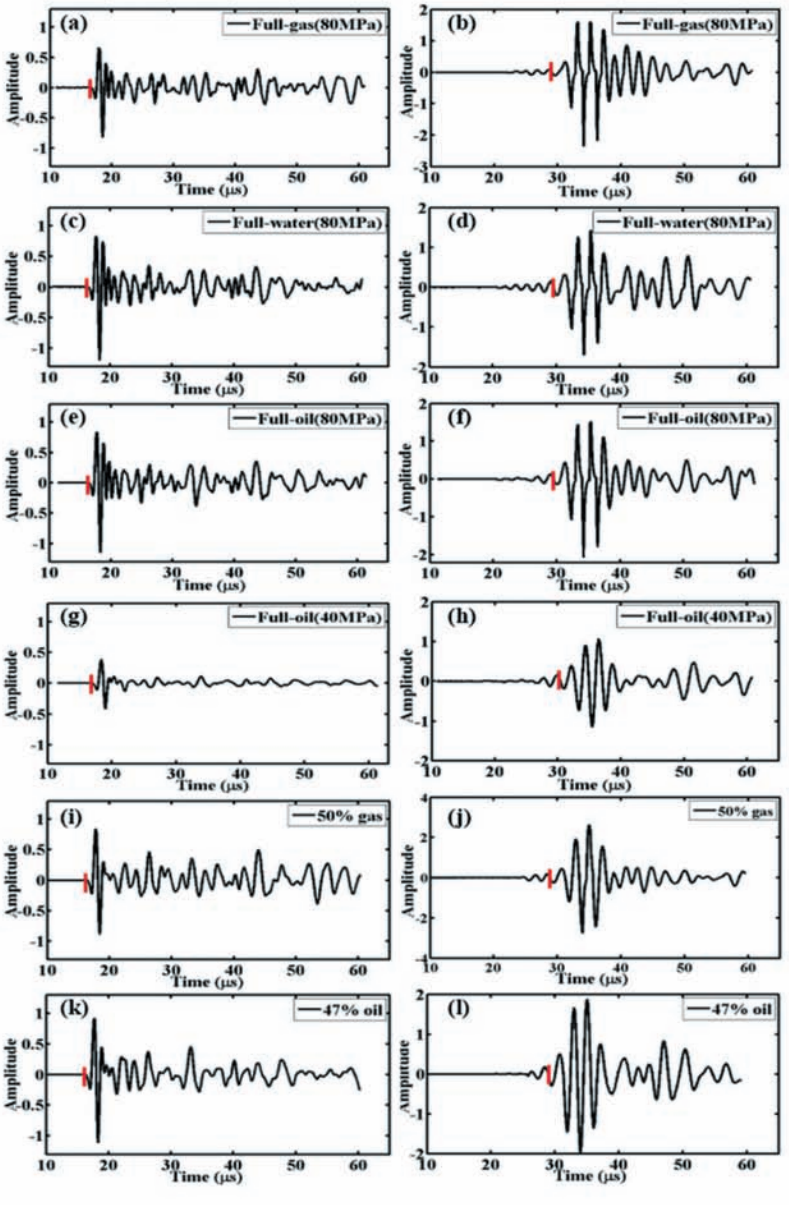

Fig. 1. Measured ultrasonic waveforms in sample F2 corresponding to compressional and shear waves are shown in the left and right columns, respectively, with different fluid types (a-b, c-d, e-f) at confining pressure of 80MPa, full oil at different confining pressures (e-f, g-h), gas saturation of 50% of the water-gas saturated state (i-j), oil saturation of 47% of the water-oil saturated state (k-l). The picked first arrivals are shown by red marks.

to vary the oil saturation. Oil saturation is controlled by weighing the sample and a small amount of air remains inside the pores at one atmosphere. Water is then injected into the sample with a pore pressure of 10 MPa. Air is light and mostly excluded from the sample during injection. The very small amount of remained air is compressed and dissolved in water at 10 MPa and can be neglected.

Measurements

Waveforms are recorded for each sample at the tested pressures and temperatures. Fig. 1 shows the waveforms of the measured ultrasonic signals in sample F2 under different experimental conditions. For the same rock, variations in fluid types, confining pressure, and saturations have affected the wave arrivals and amplitudes.

P- and S-wave velocities are obtained according to the picked first arrivals from the waveforms. Results are shown in Fig. 2 at respectively the full-gas, full-oil and full-water saturation conditions. There is noise preceding the first S arrival (it consist of weak P-wave oscillations excited by the source). The first S arrival is strong compared to the noise in most cases. The zero-crossing point followed by the first set of strong positive amplitudes is picked as the S-wave arrival. Signals from the aluminum standard can be used to control the first-arrival picking procedure (similar first oscillations of S-waves can be obtained by comparing to the aluminum standard). The measurement process is repeated several times to ensure the information from the recorded waveforms reliable. The S-wave velocity at full-oil or full-water saturation condition is lower than that at full gas saturation, the opposite to the trend of P-wave velocity.

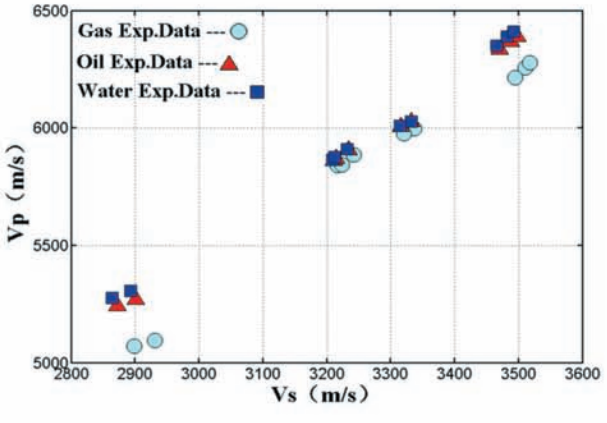

Fig. 2. P-wave velocity (V_p) as a function of S-wave velocity (V_s) for 10 carbonate specimens at full-gas, full-oil and full-water saturation conditions.

ATTENUATION ANALYSIS AND ITS SENSITIVITY TO RESERVOIRS

Estimation of the quality factor

Methods to estimate the P-wave attenuation (inverse quality factor, Q^{-1}) based on waveforms include the amplitude decay method (Tonn, 1991), the peak frequency-shift method (Zhang and Ulrych, 2002), the central frequency-shift method (Quan and Harris, 1997) and the spectral ratio method (e.g., Picotti and Carcione, 2006; Liu et al., 2010). The spectral ratio method has been used to estimate the attenuation of ultrasonic experiments (Toksöz et al., 1975; Lucet and Zinszner, 1992). In the rock tests, the transmitting and receiving transducers are located at the two ends of the cylinder specimen. The main energy propagates along the cylinder axis and can be approximated as plane waves for attenuation analysis.

The amplitude of a plane elastic wave in a reference material and the rock sample can respectively be expressed as

$$A_1(f,x) = G_1(x)e^{-\alpha_1(f)x}e^{-i(2\pi ft-k_1x)} \quad , \tag{1}$$

$$A_2(f,x) = G_2(x)e^{-\alpha_2(f)x}e^{-i(2\pi ft-k_2x)} \quad , \tag{2}$$

where the subscripts $j = 1, 2$ denote a reference material and rock sample respectively, $A_j\,(f, x)$ are frequency-dependent amplitudes, $G_j\,(x)$ are the geometrical factors that includes the wave geometrical spreading, internal reflections, etc., x is the distance, $\alpha_j\,(f)$ are the frequency-dependent attenuation factors, f is the frequency, k_j are the wave-numbers and i is the imaginary unit (e.g., Carcione, 2014). For convenience, since the measurement distance is fixed, in the following we use a notation with only the frequency dependence.

By taking the logarithm of the ratio of the modules of eq. (1) and eq. (2), we obtain

$$\ln\left(\frac{|A_1(f)|}{|A_2(f)|}\right) = \left(\alpha_2(f)-\alpha_1(f)\right)x + \ln\frac{G_1(x)}{G_2(x)} \quad . \tag{3}$$

By substituting the relationship $\alpha = (\pi f)/(QV)$ eq. (3), we have

$$\ln\left(\frac{|A_1(f)|}{|A_2(f)|}\right) = \left(\frac{\pi f}{Q_1V_1}-\frac{\pi f}{Q_2V_2}\right)x + \ln\frac{G_1(x)}{G_2(x)} \quad , \tag{4}$$

where V is the wave velocity.

If the reference medium is lossless, eq. (4) becomes

$$\ln\left(\frac{|A_1(f)|}{|A_2(f)|}\right) = -\frac{\pi f}{Q_2 V_2}x + \ln\frac{G_1(x)}{G_2(x)} \quad . \tag{5}$$

Eq. (5) is the formulation to estimate Q^{-1} of a plane wave. In order to estimate wave attenuation, eq. (5) is used to obtain the corresponding Q^{-1} at each frequency in the main energy band. The least squares method is used to estimate the equivalent Q^{-1} in the frequency band.

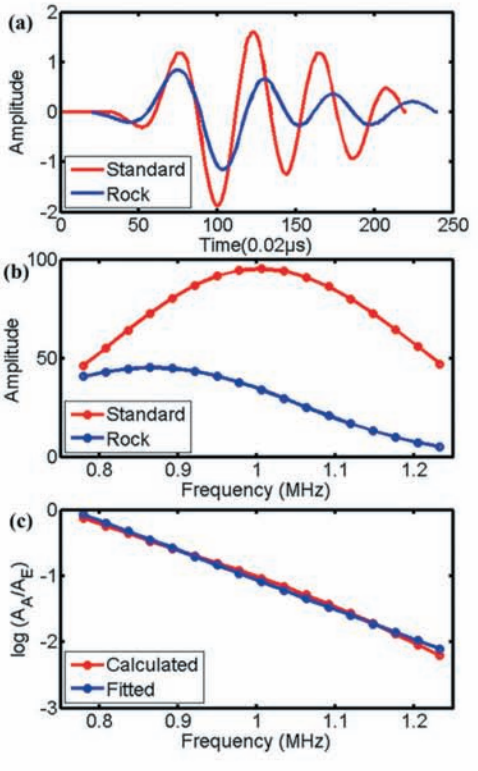

Fig. 3. Q estimation by using the spectral ratio method. (a) P-wave waveforms in rock and aluminum; (b) Spectra of the two waveforms; (c) Least squares fitting on the logarithm of the spectral ratio of A_R (wave amplitude in rock) and A_S (wave amplitude in aluminum standard).

By using the same source as that in the rock samples, the waveforms of P-waves in aluminum are recorded. Aluminum is selected as a reference material due to its virtue of a very high quality factor. This spectral-ratio method is based on a comparison between the pulses observed in a reference material and carbonate sample. We used the 4-8 periods of oscillations after the first arrival in the spectral ratio analysis. Considering a single period is not reliable because of the rock heterogeneity. Fig. 3a gives the P-wave waveforms in the rock sample and aluminum standard, where the minor effects of reverberation are removed. The spectrum of P-waves are given in Fig. 3b and the ratio of the spectra of the two materials are given together with the least squares fitting results in Fig. 3c.

Experimental results of attenuation and velocity in carbonate rocks

P-wave attenuation estimations by using the central frequency-shift (CFS) and spectral ratio (SR) method in sample A1 are shown in Fig. 4. For the two methods, the trend of the estimated attenuation varying with differential pressure ($P_d = P_c - P_p$) are similar, and at the same differential pressure, the two values of P-wave attenuation estimations are very close. The estimated results of attenuation can be related to the complexity and diversity of mineral, fabric, lithology and pore structure in different rocks, and also to the different experimental set-ups and estimation methods, however, the trend and characteristics of measured attenuation dependences of pressure are consistent with those in literature (Agersborg et al., 2008; Guo et al., 2009).

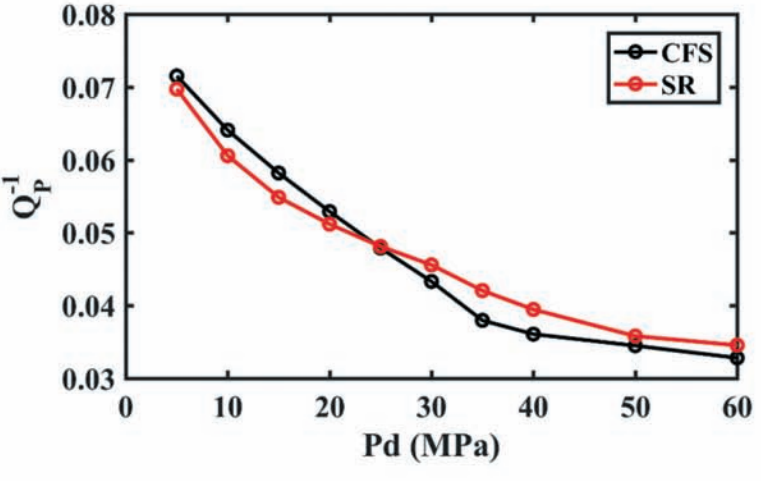

Fig. 4. P-wave attenuation estimations by using the central frequency-shift (CFS) method and the spectral ratio (SR) method in sample A1.

For limestone samples, the velocities and attenuations varying with differential pressure are shown in Fig. 5, Both the P- and S-wave velocities increase with increasing differential pressure, while the wave attenuation decreases. The major cause is that the micro-cracks tend to close when confining pressure increases while pore pressure keeps constant, which also increases the elastic moduli of the dry rock skeleton. In addition, the closure of micro-cracks and grain contacts hinders the occurrence of wave-induced local fluid flow in rocks, and weakens the scattering effects, both of which cause the decrease of compressional wave attenuation.

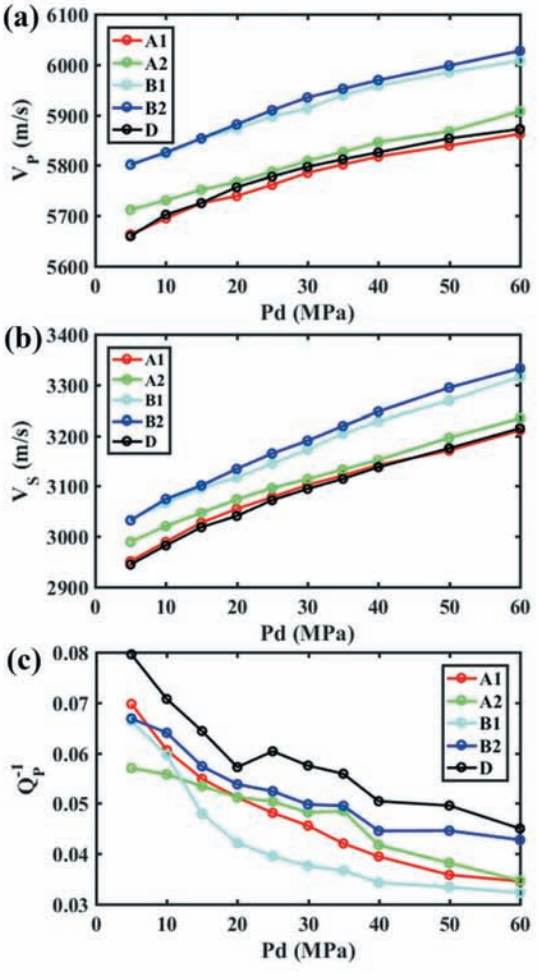

Fig. 5. P-wave velocity (a), S-wave velocity (b) and P-wave attenuation (c) as a function of differential pressure in limestone samples at full-oil saturation (with a pore pressure of 10 MPa and a temperature of 140°C).

Similar data characteristics and trend can be observed for dolomite samples, as is shown in Fig. 6. For the dolomite samples with a porosity around 0.05, Q^{-1} decreases from 0.07 (Q = 14) to around 0.05 (Q = 20) when the differential pressure increases from 10 MPa to 70 MPa. Figs. 5 and 6 show that between the samples with similar porosities, the difference in velocity is small, and the difference in P-wave inverse quality factor is larger. Samples with relatively higher porosities have higher inverse quality factors.

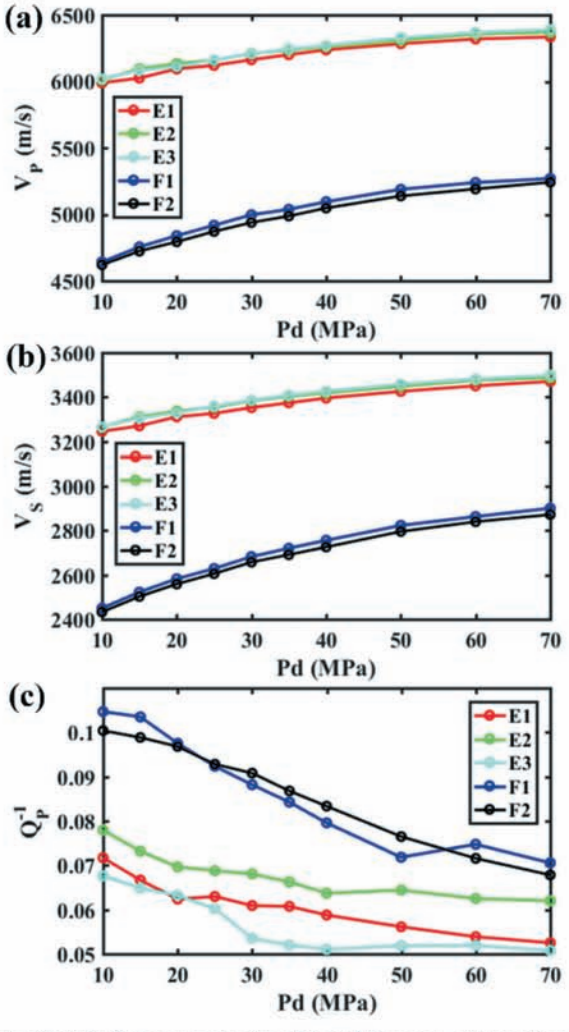

Fig. 6. P-wave velocity (a), S-wave velocity (b) and P-wave attenuation (c) as a function of differential pressure in dolomite samples at full-oil saturation (with a pore pressure of 10 MPa and a temperature of 140°C).

Fig. 7 gives the P-wave velocity, S-wave velocity and P-wave attenuation as a function of gas saturation in gas/water partial-saturation experiments for 5 dolomite samples.

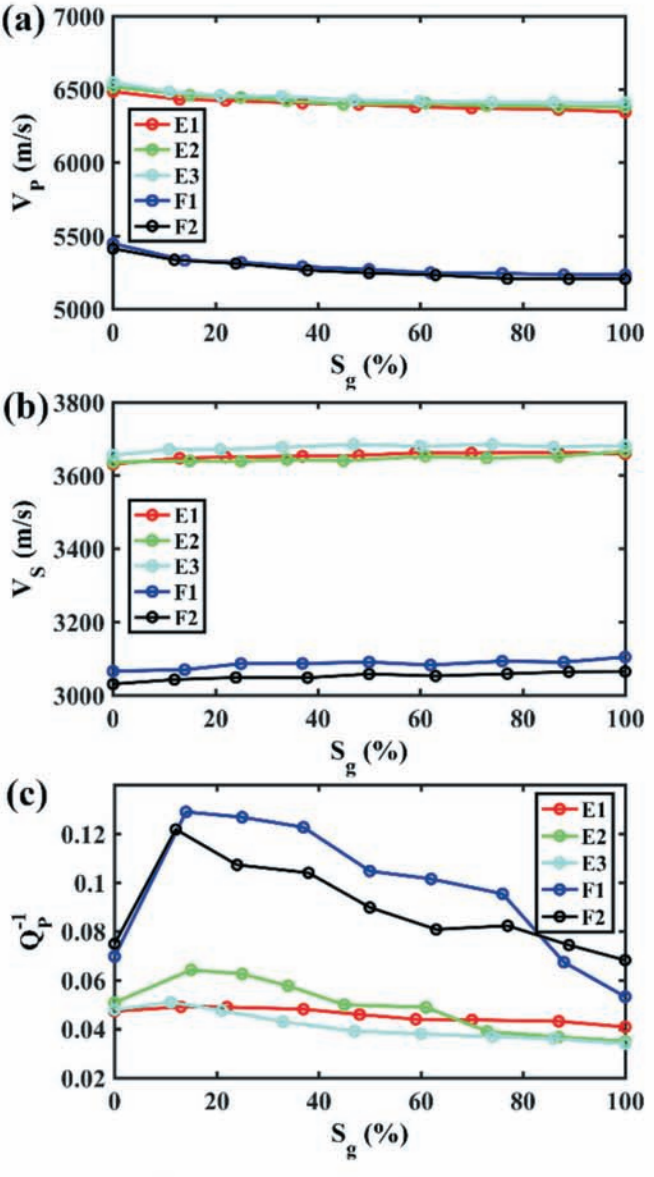

Fig. 7. P-wave velocity (a), S-wave velocity (b) and P-wave attenuation (c) as a function of gas saturation in gas/water partially-saturated samples (with a confining pressure of 80 MPa, a pore pressure of 10 MPa and a temperature of 20°C).

Fig. 8 gives the P-wave velocity, S-wave velocity and P-wave attenuation as a function of oil saturation in oil/water partial-saturation experiments. With the increase of gas saturation, the P-wave velocities gradually decrease, while the S-wave velocities increase due to the decrease

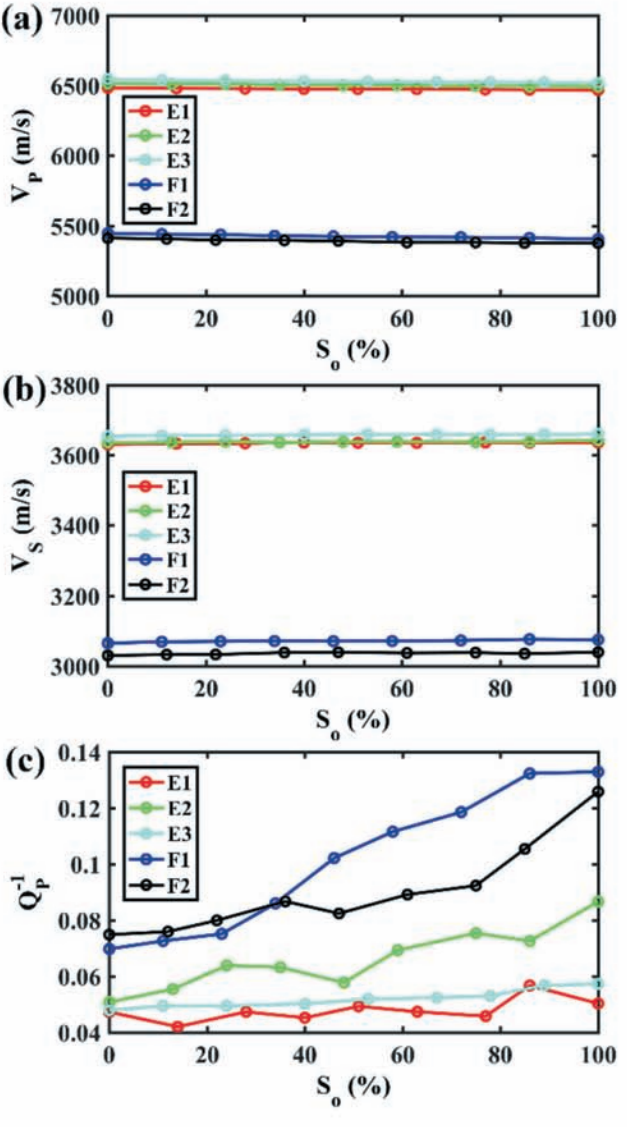

Fig. 8. P-wave velocity (a), S-wave velocity (b) and P-wave attenuation (c) as a function of oil saturation in oil/water partially-saturated samples (with a confining pressure 80 MPa, a pore pressure of 10MPa and a temperature of 20°C).

in bulk density and the fact that the shear modulus remains constant. Q_P^{-1} increases with gas saturation in the range 0-10%. It reaches a peak at around 15% gas saturation and then decreases with gas saturation in the partially-saturated rocks (the same effect has been found at seismic frequency band [Carcione et al. (2006), Fig. 7] and sonic frequency band [Cadoret et al. (1982), Fig. 2]. The P-wave shows a strongest dissipation in the gas saturation range 0-20%. Due to the low-porosity and low-permeability of the carbonate samples, the patchy saturation will also occur at the microscopic scale, causing the saturation-dependent attenuation in ultrasonic band. In the oil/water partially-saturated samples, the P-wave velocities slightly decrease with increasing oil saturation, while the S-wave velocities almost remain constant for samples E1, E2 and E3. Attenuation increases gradually with oil saturation. Samples F1 and F2 have high attenuation and low velocities, while samples E1, E2 and E3 have low attenuation and correspondingly high velocities.

In order to investigate the corresponding contribution of porosity and saturation on attenuation, a regression analysis is performed, as shown in Fig. 9, and the results can be expressed as $Q_P^{-1} = 0.021 + 0.694y_1 - 0.0029y_2$ where y_1 and y_2 denote porosity and saturation, respectively. The effect of porosity on attenuation is much more significant than that of saturation.

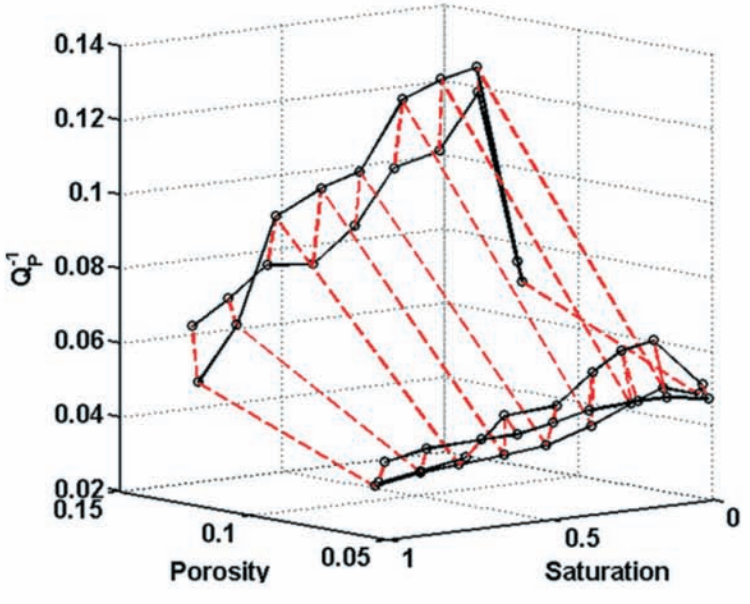

Fig. 9. Regression analyses on the effects of porosity and fluid saturation on P-wave attenuation.

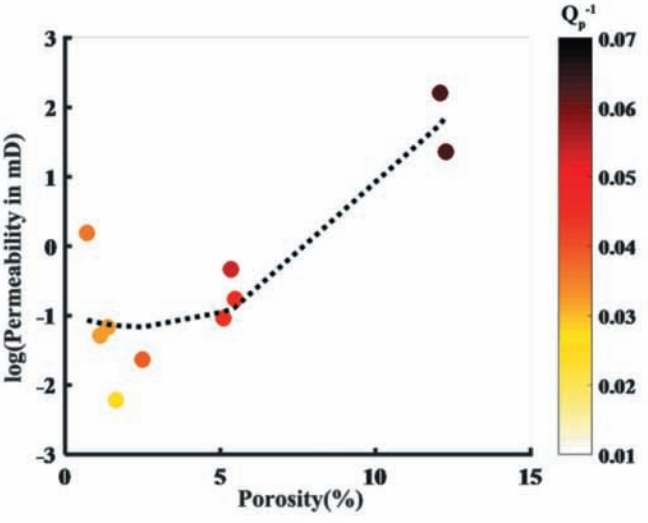

Fig. 10. Cross-plot of porosity and permeability versus P-wave attenuation at full gas-saturation.

Fig. 10 shows the cross-plot of porosity and permeability versus P-wave attenuation of the ten rock samples at full gas-saturation with confining pressure 80 MPa and pore pressure 10 MPa. Both the P-wave attenuation and rock permeability increase with increasing porosity. Fig. 11 shows the P-wave attenuation at full-gas saturation with confining pressure 80 MPa and pore pressure 10 MPa as a function of porosity and permeability, respectively. The linear fits describe the variations of P-wave attenuation versus increasing porosity and permeability.

Sensitivity analysis on rock physics parameters to porosity and permeability

By selecting the rock physics parameters/indicators which is the most sensitive to reservoir porosity and permeability, reservoir identification can then be performed on the data volume of the selected parameters.

Porosity significantly affects the mechanical and hydraulic properties of the rocks. Permeability and saturation are closely associated with rock porosity. We sort the samples into two categories according to porosity Φ, i.e., $\Phi < 3$ %, and $\Phi > 5$ % (In Table 1, five samples have a porosity < 3%, and the others have a porosity > 5%. The parameter sensitivity of the two porosity ranges is then investigated accordingly). The sensitivity to porosity and permeability of rock parameters is tested.

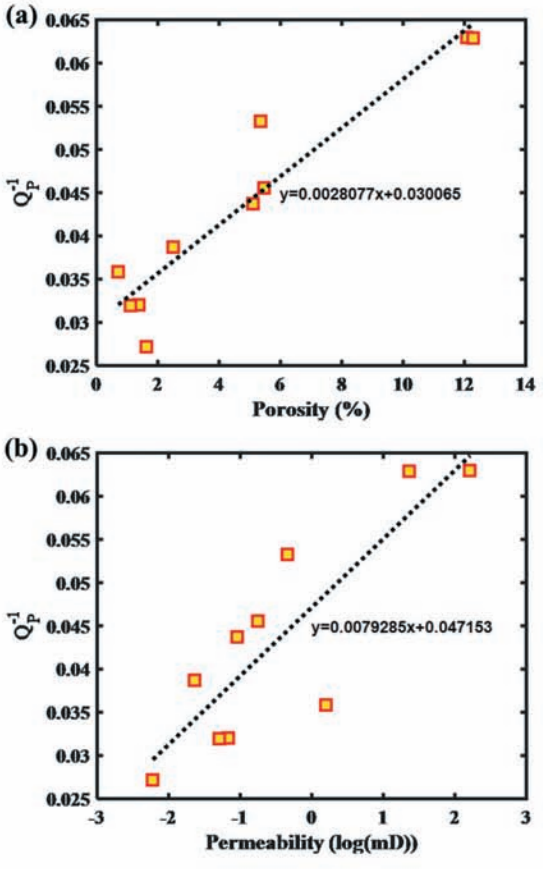

Fig. 11. Cross-plots of P-wave attenuation versus porosity (a) and permeability (b).

In order to find the most sensitive parameters to porosity or permeability in a specific porosity range of rock samples, the sensitivity of a rock parameter (A) is defined as the ratio of the absolute difference between the mean value and the value at the minimal porosity or permeability to the value at the minimal porosity or permeability in that range. The sensitivity represents the relative variation of the measured parameter according to the porosity or permeability change, which can be expressed as

$$X = \left| A_{mean} - A_{\min} \right| / A_{\min} \ , \tag{6}$$

where A_{mean} and A_{min} are the mean value and the value at the minimal porosity or permeability in the data set.

Eq. (6) indicates the relative variation of a rock parameter (A) which occurs when the rock porosity changes in the analyzed porosity range. $|A_{mean}-A_{min}|$ indicates the amplitude of the absolute variations of the parameter A in the porosity range. A larger relative variation of $|A_{mean}-A_{min}|/A_{min}$ denotes a higher sensitivity of the parameter to the porosity change in the porosity range.

Figs. 12 and 13 are the sensitivities of density (Den), P-wave velocity (Vp), S-wave velocity (V_S), the ratio of P-wave velocity to S-wave velocity (Vp/Vs), Lame coefficients (λ 、 μ) and P-wave inverse quality factor ($1/Q$) to porosity and permeability for the two categories of carbonate samples, respectively. It is shown that the Lamé coefficients (λ 、 μ) and P-wave attenuation are the most sensitive ones to rock porosity and permeability for porosities greater than 5%, however for low porosity rocks (Φ < 3 %), P-wave attenuation is better than the Lamé coefficients.

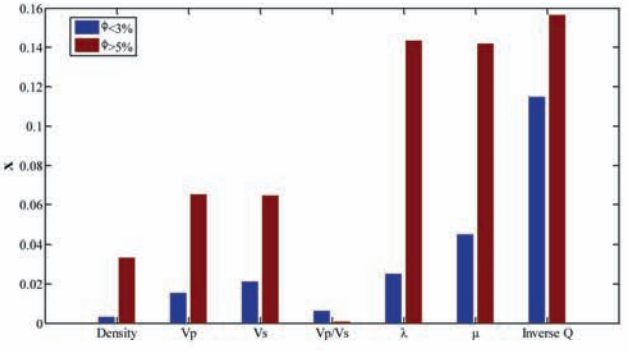

Fig. 12. Sensitivities of rock physics parameters to porosity in carbonates.

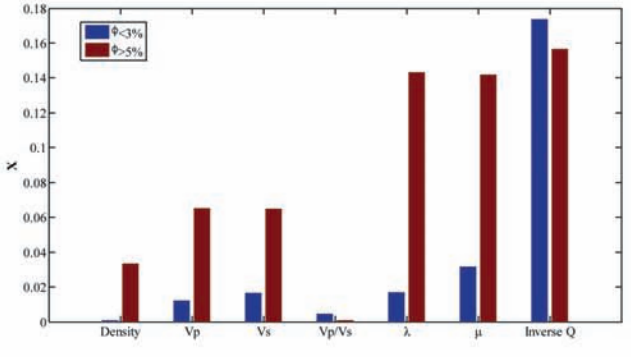

Fig. 13. Sensitivities of rock physics parameters to permeability in carbonates.

RESERVOIR IDENTIFICATION WITH SEISMIC ATTENUATION

As the most sensitive indicator, P-wave attenuation can be directly used for reservoir characterization. Inverse quality factors can be estimated from pre-stack common midpoint (CMP) gathers, or a post-stack single trace.

The workflow for estimating the inverse quality factor from the post-stack seismic data is shown in Fig. 14. The generalized S transform (Stockwell et al., 1996; Stockwell, 2007; Sahu et al., 2009) is performed on the post-stack seismic data for the time-frequency spectrum. Different from attenuation estimation for transmitted waves, for reflected waves spectral ratio method can be used to estimate Q^{-1} by comparing the amplitude spectra at the first arrival time t_1 with that at the second arrival time t_2. In the S transform, the Gaussian window is chosen for analysis. The spectra at t_1 and t_2 respectively correspond to the two adjacent events of reflected waves. The algorithm of the estimation of Q^{-1} is given by Zhang and Ulrych (2002), which can be expressed as

$$A_r = \ln\left[\frac{A_{E2}(f,t_2)}{A_{E1}(f,t_1)}\right] = -\frac{\pi(t_2-t_1)}{Q}f \quad , \tag{7}$$

where A_r is the spectral ratio. A_{E1} and A_{E2} are the amplitude spectra of the two events, respectively. Zhang and Ulrych (2002) demonstrated that Q estimation from prestack seismic data is superior to poststack seismic data, due to the processing biases of poststack data. On the other hand, it is also shown in Zhang (2008) that the approach is feasible for estimating Q from either prestack or poststack seismic data, where an example of post-stack Q estimation was given. Previous studies on Q estimation from the post-stack seismic data can be found in Dasios et al. (1998), Wang (2004) and Li et al. (2006). The applications of the spectral ratio method in Q estimation from post-stack surface seismic data can be found in White (1992) and Nunes et al. (2011).

The processing of post-stack data slightly biases the Q-frequency information from the original data. However, in the deep carbonate strata, effects from the data of far-offsets are weak, and the stacked data mainly contains the information from those wave paths at small offsets. The post-stack data mainly reflect the rock/reservoir properties at the locations around the analyzed position. The final Q estimation result at the position is actually the spatial average of the true Qs in a small zone around the position, which can be used to estimate the lateral Q variations in the target strata, and then helps permeability prediction and reservoir identification by incorporating the experimental empirical relations.

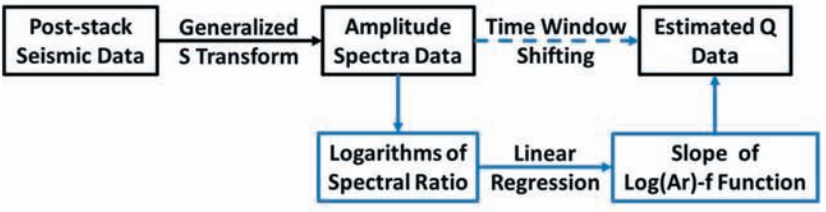

Fig. 14. Workflow for estimating attenuation from post-stack seismic data by the spectral-ratio method.

Fig. 15a shows the seismic wave data of a single trace in the target formation. Correspondingly, the S-transform time-frequency spectrum and the amplitude spectrum are respectively given in Figs. 15b and 15c. By use of S-transform, the time-frequency spectrum is produced, and the amplitude spectrum is given at each time of the trace data, with which the logarithms of spectral ratio are calculated and attenuation is then estimated.

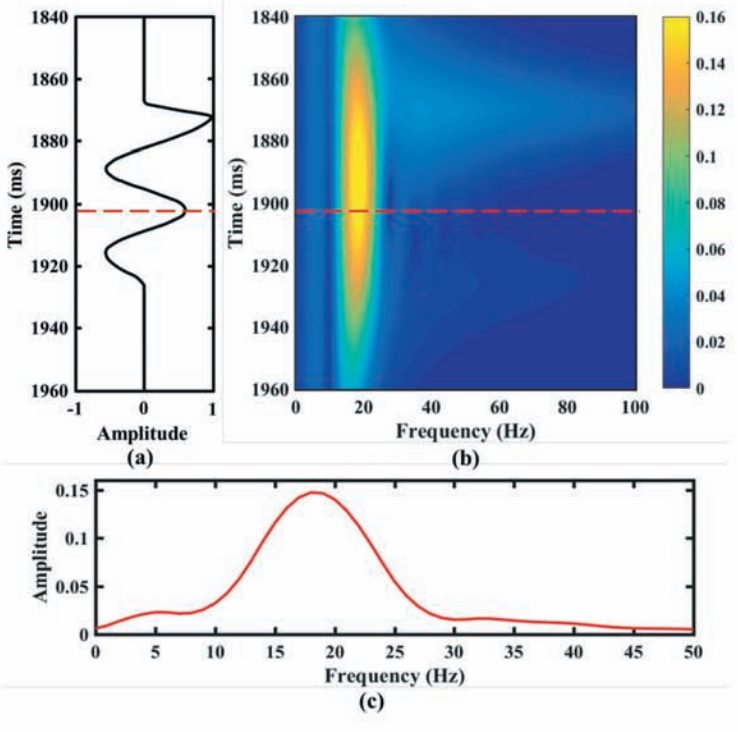

Fig. 15. The seismic trace data in the target formation (a) and the corresponding S-transform time-frequency spectrum (b) and amplitude spectrum at 1902 ms (c).

A work area is selected here where the target stratum of natural gas reservoirs mainly consists of limestone rocks with pores resulting from dissolution and rare clay. The area is located on the carbonate terraces at the target formation, which is within the Jurassic system. The samples in rock tests have very similar textures (grain-rich carbonates) as the reservoir rocks from the target formation. The sample minerals are almost pure dolomite or limestone with rare clay, which also agree with the reservoir rocks. A section profile of 2D seismic line crossing two gas production wells (Met22 and Met23) is shown in Fig. 16.

Well-log interpretation results and gas production reports indicate that there are high-quality reservoirs at the both wells. Well Met22 had a high gas production rate of more than 6×10^5 m^3 per day and well Met23 produces gas in the upper part of the target formation and brine around the bottom.

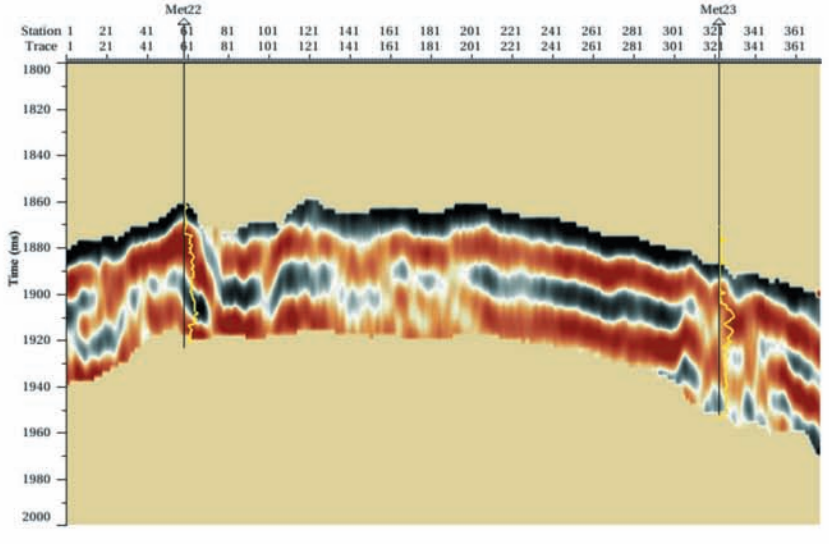

Fig. 16. Seismic section profile of a 2D line crossing the two gas production wells for the target formation. The yellow curves give the porosity data by the well-log interpretation.

Fig. 17 shows various log curves observed at the two wells, including sonic log data, density, water saturation, porosity and permeability. High-porosity intervals are observed on the porosity log curves in the target formation (around 2665-2760 m depth at well Met22 and 2780-2890 m depth at well Met23). It is also that the gas saturation in the rocks around the top of well Met22 is higher than that from well Met23 according to the saturation log data.

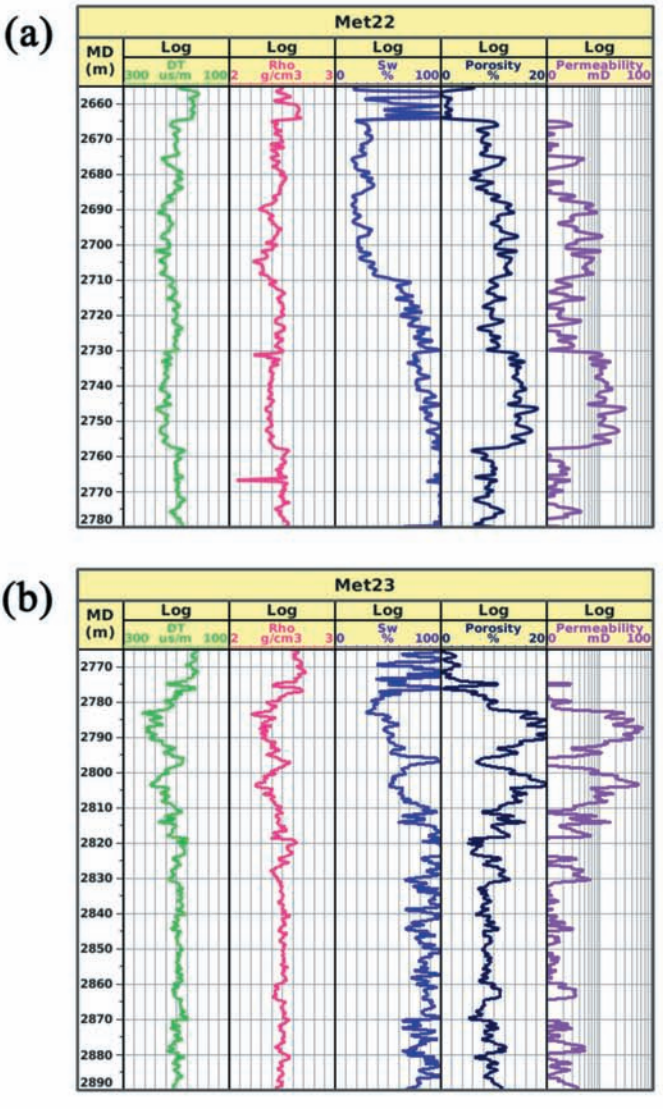

Fig. 17. Data curves of sonic log, rock density, water saturation, porosity and permeability of well Met22 (a) and Met23 (b).

The spectral-ratio method is applied on the post-stack seismic data (shown in Fig. 16) for estimating Q^{-1} in the target formation. The results are shown in Fig. 18. By comparison with the porosity log curves, the estimated

Q^{-1} sections show the spatial distribution of hydrocarbon reservoirs in the formation. Gas reservoirs at Met22 exhibit almost even P-wave attenuation from the top to bottom, while those at Met23 shows significant P-wave attenuation variations with depth.

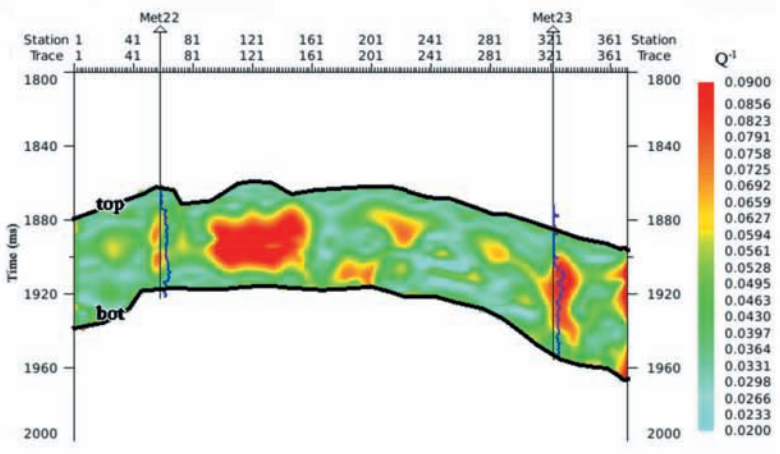

Fig. 18. The estimated Q^{-1} section of the target formation by the spectral-ratio method. The blue curves give the porosity data by the well-log interpretation.

To further investigate the attenuation characteristics versus porosity and permeability, borehole-side Q^{-1} attribute traces are extracted and analyzed, which are shown in Fig.19. The estimated Q^{-1} increases with increasing porosity and permeability.

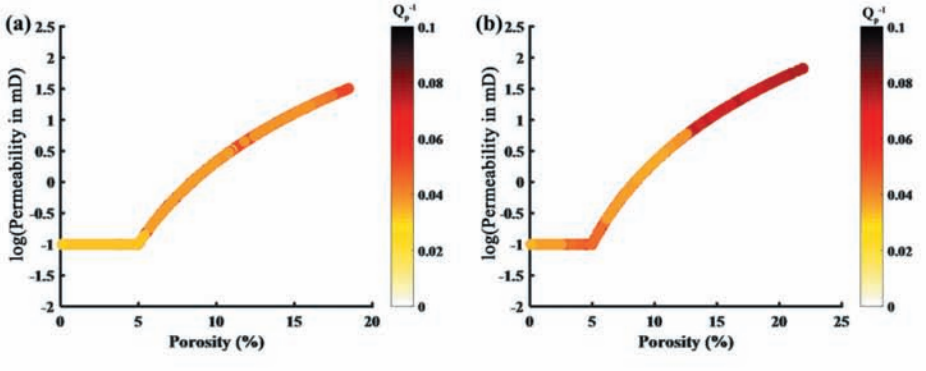

Fig. 19. Crossplots of porosity and permeability versus attenuation at Well Met22 (a) and Well Met23 (b).

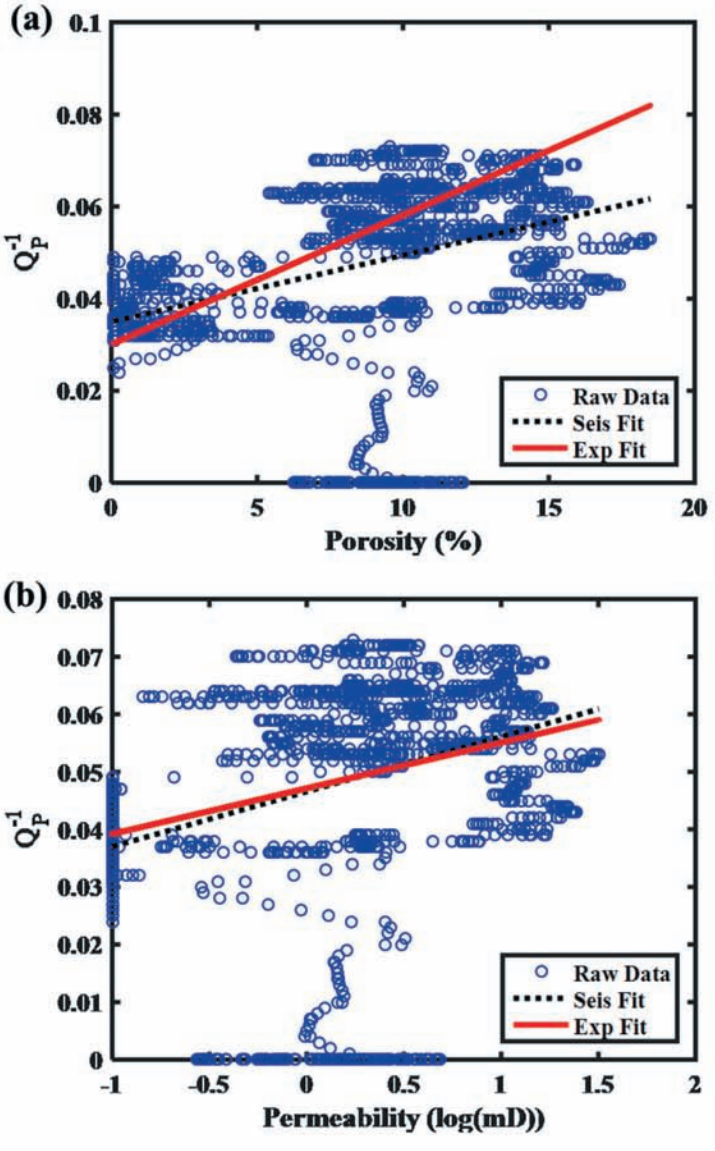

Fig. 20. Cross-plots of P-wave attenuation versus porosity (a) and permeability (b) respectively at well Met22. The red lines are the linear fitting results for the experimental data as shown in Fig. 10, which are used to invert for porosity and permeability. For the raw data, the attenuation is extracted from the seismic traces which are located beside the wells, and the porosity is given based on the well-log interpretation (by field petrophysicists). The black dotted lines are the fitting results of the scattered circle symbols from seismic analysis.

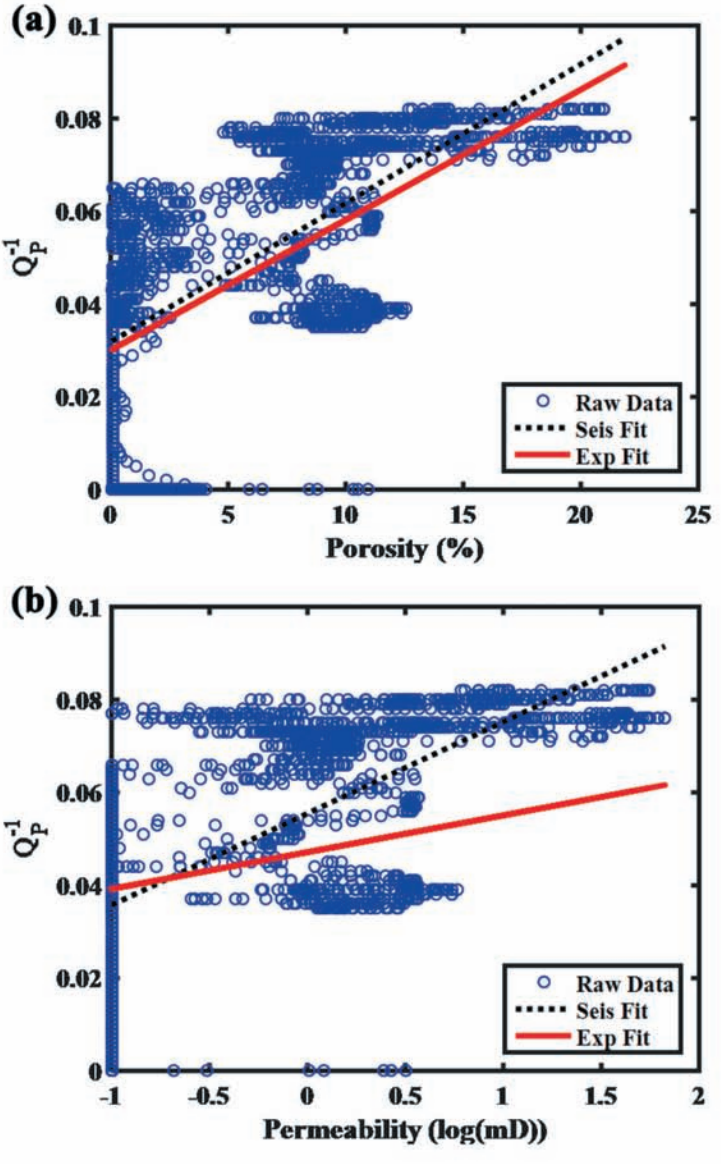

Fig. 21. Cross-plots of P-wave attenuation versus porosity (a) and permeability (b) respectively at well Met23. The red lines are the linear fitting results for the experimental data as shown in Fig. 10. For the raw data, the attenuation is extracted from the seismic traces which are located beside the wells, and the porosity is given based on the well-log interpretation (by field petrophysicists). The black dotted lines are the fitting results of the scattered circle symbols from seismic analysis.

Figs. 20 and 21 are the cross-plots of P-wave attenuation, which is estimated from the seismic data, versus porosity and permeability at well Met22 and Met23, respectively. The two empirical relationships between P-wave attenuation and porosity and permeability, which are derived from linear fittings on the experimental data, are overlapped on the two crossplots. The rock samples in the ultrasonic tests can be related to the studied reservoirs, since they have very similar textures (grain-rich; clean with rare clay; dissolution pores; reef carbonates) as the reservoir rocks from the target formation. The condition (confining pressure and temperature) in the experiments is also close to the in-situ condition of the analyzed formation. In fact, the rock permeability of the in-situ formations cannot be estimated or measured when it is less than 0.1 mD. The value of 0.1 mD is approximately assigned to all those rocks with lower permeability (they cannot be considered as effective reservoirs for hydrocarbon production). Therefore, a constraint of 0.1mD (of data range) is incorporated into the applicable empirical relationship, which is helpful for discriminating effective reservoirs from low-permeability tight rocks. In Figs. 19-21, the data with $Q^{-1} = 0$ denote rocks with very low attenuation (due to the limit of precision, it is very difficult to estimate Q at low attenuation). All the low-attenuation rocks will affect the fit relationships and cannot be ignored. This part of data is approximately considered as $Q^{-1}= 0$ in the process of identifying high-quality reservoirs. If this data is excluded of the analysis, the fit would cause an underestimation of the rock porosity and permeability.

It is interesting to find that in well Met22, the fitting results from ultrasonic experiments overestimate the P-wave attenuation in comparison with the linear fitting results between the Q^{-1} and porosity from seismic attenuation analysis, while they agree well with the fitting results between the Q^{-1} and permeability from seismic analysis, on the other hand, in well Met23, ultrasonic fitting results agree well with seismic fitting results between the Q^{-1} and porosity analysis, however they underestimate the P-wave attenuation of seismic fitting results for the Q^{-1} and the permeability case.

There are differences between the variations of ultrasonic attenuation and those of seismic attenuation as a function of porosity, since the two sets of data are obtained from different observation scales. However it is shown in Figs. 20-21 that the empirical relationships corresponding to the two scales are very similar. The trend of seismic attenuation changes versus rock porosity is consistent with that obtained at the ultrasonic band, suggesting that the related relationship can be applied in the seismic band.

For low-porosity rocks, the attenuation-saturation relation does not exist apparently. But still, the level of attenuation ($1/Q$~0.05) is relatively high. It can be deduced that rock fabric structures control the attenuation values instead of saturation changes in these tight rocks, for instance, the

squirt-flow mechanism caused by soft grain contacts. For high-porosity rocks, although there is a pronounced attenuation-saturation relation, attenuation is more sensitive to rock porosity changes than saturation. Furthermore, there exists a linear fit relationship between log permeability and porosity, both of which can be related to rock fabric structures and frame heterogeneity. Therefore, reservoir porosity and permeability can be estimated from seismic attenuation, and the fluctuations of the saturation will introduce an uncertainty on the porosity/permeability seismic predictions, especially for high-porosity rocks.

The gas/brine saturation affects the P-wave attenuation. However, this effect is weaker compared to those caused by the porosity variations. Porosity dominates the attenuation characteristics when porosity and gas/brine saturation simultaneously change in the formation. The effects of saturation are neglected when we use the relationships between attenuation and porosity to predict high-quality reservoirs.

Therefore, the experimental empirical relationships between Q^{-1} and porosity and permeability are used in seismic attenuation data to estimate reservoir porosity and permeability. Fig. 22 shows the estimated porosity and logarithm of permeability 2D sections, which directly indicates the good quality reservoir rocks. Both wells show good quality in the porosity and permeability sections, and well Met23 shows better potential than well Met22, especially for the upper part of the formation around this well.

Different from the attenuation-porosity relation, the attenuation-permeability relation is more complicated and can hardly be described by the suggested linear relation, especially for the rocks with a permeability >1000mD. The experimental linear relation applies to the range of 0.001-1000 mD (see Fig. 11). Consequently, by use of this empirical relation, the workflow could cause wrong interpretations when permeability >1000 mD. Therefore, the linear relation cannot be used to predict rock permeability from seismic data outside the range of 0.001-1000 mD. However, it is still useful to identify the high quality reservoirs since it can be applied to rocks with a permeability up to 1000 mD (even for rocks with a permeability >1000 mD, the relation can be used to discriminate between low and high permeability rocks).

CONCLUSIONS

Ultrasonic P- and S-wave waveforms of ten carbonate samples are measured at in-situ conditions. Correspondingly P-wave attenuation is estimated by a spectral-ratio method. Analysis on the elastic wave velocities and attenuation characteristics of the experimental data shows that both wave velocities and attenuation are strongly influenced by rock porosity,

fluid type, saturation and confining pressure. P-wave velocity increases with increasing confining pressure and with decreasing gas- and oil-saturation. S-wave velocities increase with increasing gas- and oil-saturation. With increasing confining pressure, P-wave attenuation gradually decreases. When carbonate rocks are saturated with oil and water, P-wave attenuation increases with increasing oil saturation. When the carbonate rocks are partially saturated with gas and water, the attenuation variation features are different from those in rocks saturated with oil and water. P-wave attenuation reaches the peak value in the gas saturation range of approximately 10-20%.

The relationships between P-wave attenuation (Q^{-1}) and porosity and permeability are analyzed and empirical linear relations are obtained. The sensitivity of the rock-physics properties/indicators to porosity and permeability are investigated by sorting the carbonate samples into two categories according to porosity. The results show that P-wave attenuation is one of the most sensitive indicators.

Based on experimental analysis, we identify actual hydrocarbon reservoirs by seismic attenuation analysis. P-wave attenuation is estimated by using spectral-ratio method based on a generalized S transform. In comparison with the log interpretation results of porosity and permeability of in-situ rocks, linear fittings are performed on the extracted attenuation attributes and porosity and log permeability, which are in good agreement with the experimental empirical relationships. The linear fitting relationships from experimental analysis are successfully applied on seismic attenuation data to identify high-quality reservoir rocks. The methodology can be tested in other carbonate reservoirs to obtain the relation between wave attenuation and rock porosity/permeability, which is applicable in guiding quantitative seismic interpretation for heterogeneous hydrocarbon reservoirs.

It has been widely accepted that the intrinsic wave velocity dispersion can be strictly related to attenuation and vice versa. However, in the actual application of seismic exploration, it is very difficult to extract the velocity dispersion from field data. Wave velocity at a fixed frequency can be easily obtained but is not sensitive to reservoir porosity as attenuation. The empirical relationships between P-wave attenuation and porosity/ permeability from rock experiments can be effective in field applications. In future studies, to develop a new method for extracting velocity dispersion from field data will be a challenge, which has a great potential.

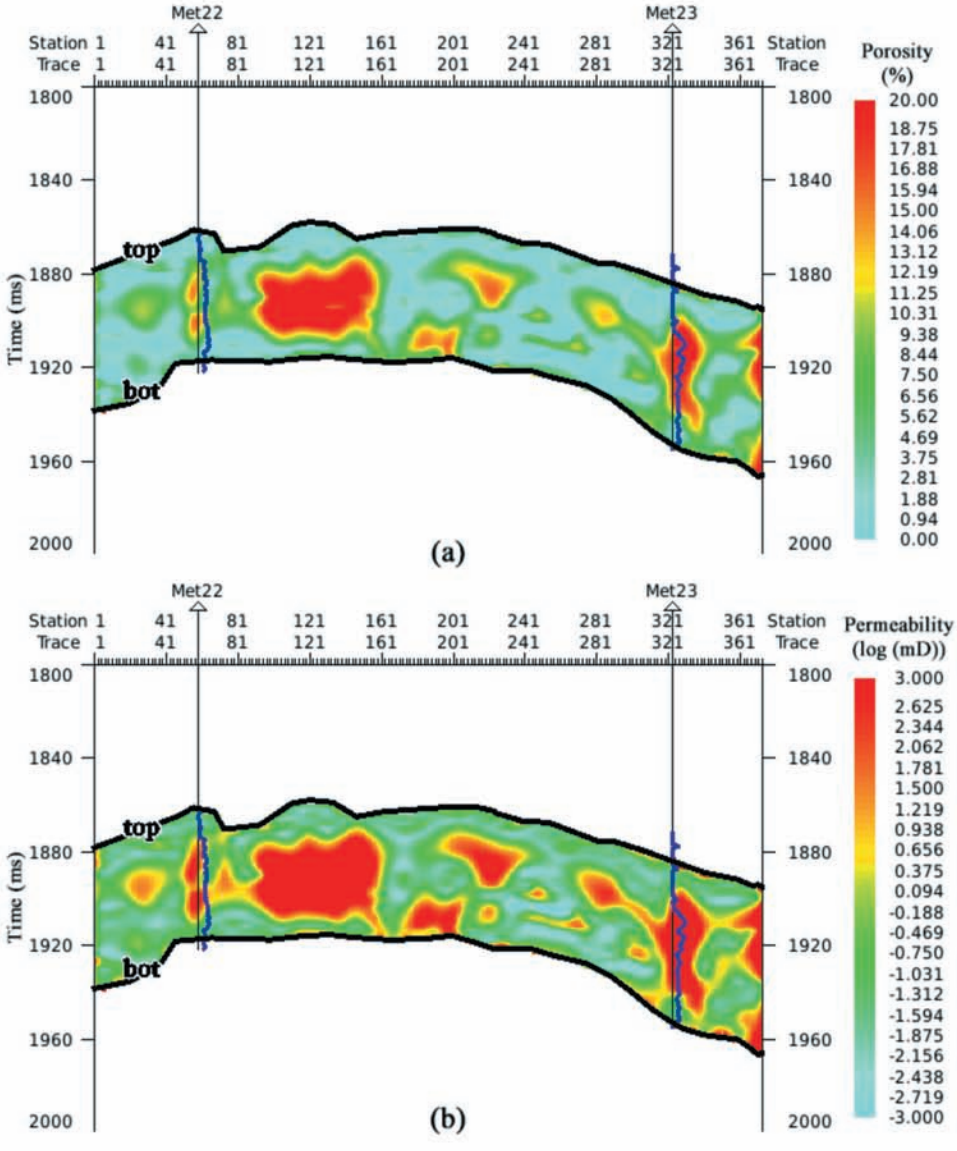

Fig. 22. Estimated porosity and logarithm of the permeability based on seismic attenuation analysis.

ACKNOWLEDGEMENTS

Zhaobing Hao and Xiangyang Wu helped performing ultrasonic measurements on the carbonate samples. The discussions with Jiong Liu and Tiansheng Chen are insightful. The first author is grateful to the support of "the Distinguished Professor Program of Jiangsu Province, China", "the Fundamental Research Funds for the Central Universities, China" and the open fund of the State Key Laboratory of the Institute of Geodesy and Geophysics, CAS (SKLGED2017-5-2-E)

REFERENCES

Adam, L., Batzle, M., Lewallen, K. and van Wijk, K., 2009. Seismic wave attenuation in carbonates. J. Geophys. Res., 114(B6): 258-266.

Agersborg, R., Johansen, T.A., Jakobsen, M., Sothcott, J: and Best, A., 2008. Effects of fluids and dual-pore systems on pressure-dependent velocities and attenuations in carbonates. Geophysics, 73(5): N35-N47.

Ba, J., Carcione, J.M., Cao, H., Du, Q., Yuan, Z. and Lu, M., 2012. Velocity dispersion and attenuation of P-waves in partially-saturated rocks-Wave propagation equations in double-porosity medium. Chin. J. Geophys. (in Chinese), 55: 219-231.

Ba, J., Du, Q., Carcione, J.M., Zhang, H. and Müller, T.M., 2015. Seismic Exploration of Hydrocarbons in Heterogeneous Reservoirs: New Theories, Methods and Applications. Elsevier Science Publishers, Amsterdam.

Ba, J., Xu, W., Fu, L., Carcione, J.M. and Zhang, L., 2017. Rock anelasticity due to patchy saturation and fabric heterogeneity: A double double-porosity model of wave propagation. J. Geophys. Res.-Solid Earth, 122: 1949-1976.

Ba, J., Zhao, J., Carcione, J.M. and Huang, X., 2016. Compressional wave dispersion due to rock matrix stiffening by clay squirt flow. Geophys, Res. Lett., 43: 6186-6195. doi:10.1002/2016GL069312.

Baechle, G.T., Colpaert, A., Eberli, G.P. and Weger, R.J., 2008. Effects of microporosity on sonic velocity in carbonate rocks. Geophysics, 27: 1012-1018.

Baechle, G.T., Weger, R.J., Eberli, G.P., Massaferro, J.L. and Sun, Y., 2005. Changes of shear moduli in carbonate rocks: Implications for Gassmann applicability. The Leading Edge, 24: 507-510.

Bouchaala, F., Ali, M.Y. and Farid, A., 2014. Estimation of compressional seismic wave attenuation of carbonate rocks in Abu Dhabi, United Arab Emirates. Compt. Rend. Geosci., 346: 169-178.

Cadoret, T., Mavko, G. and Zinszner, B., 1998. Fluid distribution effect on sonic attenuation in partially saturated limestones. Geophysics. 63: 154-160.

Carcione, J.M., Helle, H.B. and Pham, N.H., 2003. White's model for wave propagation in partially saturated rocks. Comparison with poroelastic numerical experiments. Geophysics, 68: 1389-1398

Carcione, J.M., 2014. Wave Fields in Real Media, Theory and Numerical Simulation of Wave Propagation in Anisotropic, Anelastic, Porous and Electromagnetic Media (3rd ed., extended and revised). Elsevier Science Publishers, Amsterdam.

Carcione, J.M., Picotti, S., Gei, D. and Rossi, G., 2006. Physics and seismic modeling for monitoring CO2 storage. Pure Appl. Geophys., 163: 175-207.

Chopra, S., Chemingui, N. and Miller, R.D., 2005. An introduction to this special section - carbonates. The Leading Edge, 24: 488-489.

Dasgupta, R. and Clark, R.A., 1998. Estimation of Q from surface seismic reflection data. Geophysics, 63: 2120-2128.

Dasios, A.-T., Astin, T.R. and McCann, C., 1998. Increasing confidence in seismic Q measurements: a comparison of estimates from sonic and surface seismic data. Expanded Abstr., 68th Ann. Internat. SEG Mtg., New Orleans: 1080-1083.

Eberli, G.P., Baechle, B., Anselmetti, F. and Incze, M., 2003. Factors controlling elastic properties in carbonate sediments and rocks. The Leading Edge, 22: 654-660.

Guo, M., Fu, L. and Ba, J., 2009. Comparison of stress-associated coda attenuation and intrinsic attenuation from ultrasonic measurements. Geophys. J. Internat., 178: 447-456.

Kumar, M. and Han, D., 2005. Pore shape effect on elastic properties of carbonate rocks. Expanded Abstr., 75th Ann. Internat. SEG Mtg., Houston: 1477-1480.

Li, H., Zhao, W., Cao, H., Yao F. and Shao, L., 2006. Measures of scale based on the wavelet scalogram with applications to seismic attenuation. Geophysics, 71(5): V111-V118.

Liu, J., Ba, J., Ma, J. and Yang, H., 2010. An analysis of seismic attenuation in random porous media. Sci. Chin. Phys., Mechan. Astron., 53: 628-637.

Lucet, N. and Zinszner, B., 1992. Effects of heterogeneities and anisotropy on sonic and ultrasonic attenuation in rocks. Geophysics, 57: 1018-1026.

Mahbaz, S.B., Sardar, H. and Memarian, H., 2012. Determination of a rock physics model for the carbonate Fahliyan Formation in two oil wells in sourthwestern Iran. Explor. Geophys., 43: 47-57.

Mavko, G.M. and Nur, A., 1975. Melt squirt in the asthenosphere. J. Geophys. Res., 80: 1444-1448.

Mavko, G.M. and Nur, A., 1979. Wave attenuation in partially saturated rocks. Geophysics, 44: 161-178.

Nunes, B.I.D.C., Medeiros, W.E.D., Nascimento, A.F.D. and Moreira, J.A.D.M., 2011. Estimating quality factor from surface seismic data: A comparison of current approaches. J. Appl. Geophys., 75: 161-170.

Picotti, S. and Carcione, J.M., 2006. Estimating seismic attenuation (Q) in the presence of random noise. J. Seismic Explor., 15: 165-181.

Prasad, M., Fabricius, I.L. and Olsen, C., 2005. Rock physics and statistical well log analyses in marly chalk. The Leading Edge, 24: 491-495.

Pride, S.R., Berryman, J.G. and Harris, J.M., 2004. Seismic attenuation due to wave-induced flow. J. Geophys. Res., 109(B1), B01201.

Quan, Y. and Harris, J.M., 1997. Seismic attenuation tomography using the frequency shift method. Geophysics, 62: 895-905.

Sahu, S.S., Panda, G. and George, N.V., 2009. An improved S-transform for time-frequency analysis. Advance Computing Conf., IACC 2009, Patiala, India.

Sain, R., Chen, G., Xu, S. and Payne, M.A., 2008. Carbonate rock physics: Geophysical and petrophysical pore types of carbonate rocks from an offshore carbonate field. Expanded Abstr., 78th Ann. Internat. SEG Mtg., Las Vegas: 1655-1699.

Sayers, C.M., 2008. The elastic properties of carbonates. The Leading Edge, 27: 1020-1024.

Stockwell, R.G., 2007. A basis for efficient representation of the S-transform. Digit. Sign. Process., 17: 371-393.

Stockwell, R.G., Mansinha, L. and Lowe, R.P., 1996. Localization of the complex spectrum: the S transform. IEEE Transact. Sign. Process., 44: 998-1001.

Sun, Y., 2004. Seismic signatures of rock pore structure. Appl. Geophys., 1: 42-49.

Sun, Z., Wang, H., Liu, Z., Li, Y., Zhou, X. and Wang, Z., 2012. The theory and application of DEM-Gassmann rock physics model for complex carbonate reservoirs. The Leading Edge, 31: 152-158.

Toksöz, M.N., Johnston, D.H. and Timur, A., 1979. Attenuation of seismic waves in dry and saturated rocks: I. Laboratory measurements. Geophysics, 44: 681-690.

Tonn, R., 1991. The determination of the seismic quality factor Q from VSP data: A comparison of different computational methods. Geophys. Prosp., 39: 1-27.

Vanorio, T., Scotellaro, C. and Mavko, G., 2008. The effect of chemical and physical processes on the acoustic properties of carbonate rocks. The Leading Edge, 27: 1040-1048.

Weger, R.J., Eberli, G.P., Baechle, G.T., Massaferro, J.-L. and Sun, Y.F., 2009. Quantification of pore structure and its effect on sonic velocity and permeability in carbonates. AAPG Bull., 93: 1297-1317.

Wang, Y., 2004. Q analysis on reflection seismic data. Geophys. Res. Lett., 31(17): L17606.

White, J., 1975. Computed seismic speeds and attenuation in rocks with partial gas saturation. Geophysics, 40: 224-232.

White, R., 1992. The accuracy of estimating Q from seismic data. Geophysics, 57: 1508-1511.

Winkler, K.W. and Nur, A., 1979. Pore fluids and seismic attenuation in rocks. Geophys. Res. Lett., 6: 1-4.

Winkler, K.W. and Murphy, W.F. III, 1995. Acoustic velocity and attenuation in porous rocks. In: Rock Physics and Phase Relations, Vol. 3, AGU: 20–34.

Xu, S. and Payne, M.A., 2009. Modeling elastic properties in carbonate rocks. The Leading Edge, 28: 66-74.

Xu, S. and White, R.E., 1995. A new velociy model for clay-sand mixtures. Geophys. Prosp., 43: 91-118.

Zhang, C., 2008. Seismic Absorption Estimation and Compensation. Ph.D. Thesis, The University of British Columbia, Vancouver.

Zhang, C. and Ulrych, T.J., 2002. Estimation of quality factors from CMP records: Geophysics, 67: 1542-1547.